Surface Based Decoding of Fusiform Face Area Reveals Relationship Between SNR and Accuracy in Support Vector Regression

Amnah M. Eltahir

Thesis submitted to the Faculty of the
Virginia Polytechnic Institute and State University
in partial fulfillment of the requirements for the degree of

Masters of Science
in
Biomedical Engineering and Mechanics

Stephen M. LaConte, Chair
Pamela VandeVord
Giti Khodaparast

April 11th, 2018
Blacksburg, Virginia

Keywords: fMRI, Support Vector Regression, Fusiform Face Area, Resting Stae, Functional Connectivity

Surface Based Decoding of Fusiform Face Area Reveals Relationship Between SNR and Accuracy in Support Vector Regression

Amnah M. Eltahir

(ABSTRACT)

The objective of this study was to expand on a method previously established in the lab for predicting subcortical structures using functional magnetic resonance imaging (fMRI) data restricted to the cortical surface. Our goal is to enhance the utility of low cost, portable imaging modalities, such as functional near infrared spectroscopy (fNIRS), which is limited in signal penetration depth. Previous work in the lab successfully employed functional connectivity to predict ten resting state networks and six anatomically defined structures from the outer 10 mm layer of cortex using resting state fMRI data. The novelty of this study was two-fold: we chose to predict the functionally defined region fusiform face area (FFA), and we utilized the functional connectivity of both resting state and task activation. Right FFA was identified for 27 subjects using a general linear model of a functional localizer tasks, and the average time series were extracted from right FFA and used as training and testing labels in support vector regression (SVR) models. Both resting state and task data decoded activity in right FFA above chance, both within and between run types. Our method is not specific to resting state, potentially broadening the scope of research questions depth-limited techniques can address. We observed a similarity in our accuracy cross-validation to previous work in the lab. We characterized this relationship between prediction accuracy and spatial signal-to-noise (SNR). We found that this relationship varied between resting state and task, as well as the functionality of features included in SVR modeling.

Surface Based Decoding of Fusiform Face Area Reveals Relationship Between SNR and Accuracy in Support Vector Regression

Amnah M. Eltahir

(GENERAL AUDIENCE ABSTRACT)

We used functional magnetic resonance imaging (fMRI) to predict activity in a deep brain region based on activity along the brain surface. This would increase the type of brain function a person could study using alternative methods that are less costly and easier to use, but can only detect signals along the surface. We were able to use this method to predict the fusiform face are, a region in the brain that responds more strongly to face images than other types of images. We also found a relationship between the quality of spatial information in the brain and the accuracy of predictions. This relationship differed depending on the types of brain regions were used to build the models, as well as whether the subjects were performing a task or rest scan.

Contents

List of Figures

List of Tables

Chapter 1

Introduction

Functional magentic resonace imaging (fMRI) is capable of providing anatomical information regarding brain function with high spatial resolution [1, 2]. However, data acquisition can be highly prohibitive due to high cost, operational requirements and MR patient contraindicators [3]. Less resctrictive, relatively inexpensive alternatives to fMRI include magnetoencephelography (MEG) and functional near infrared (fNIRS). Unfortunately, these modalities have low spatial resolution and are restricted to the most superficial layers of cortex. The limitations in these neuroimaging approaches may be addressed through a multi-modal approach. In this study, we attempted to build on a method previously established in the lab for overcoming the spatial limitations in fNIRS using fMRI data by decode deep brain regions using only voxels in the cortical surface.

1.1 fMRI

Blood oxygenation level-dependent (BOLD) fMRI is a non-invasive tool for measuring hemodynamic correlates of brain activity [1]. It enables us to represent vascular changes as voxels of time series, mapping activation onto a subject's anatomy. Since the early 1990's this technique has been used to answer a wide range questions pertaining to the physiology and psychology of humans, both in health and disease.

Typical fMRI studies observe either intrinsic brain activation during "resting state" or extrinsicly driven activation during "task" [4, 5]. Task based fMRI is a useful tool for identifying brain regions required for different specific cognitive demands. Resting state fMRI exploits spontaneous fluctuations across the brain to study regional interactions of spatially independent regions, often with the goal of revealing functionally linked resting state networks (RSNs) [6, 7, 8]. The level of time series co-activation within these RSNs describes the strength of their functional connecitvity. While resting state fluctuations may persist

during cognitive tasks, task fMRI is not typically used to directly characterize resting state functional connectivity, as the extrinsicly driven response dominates the measured BOLD response.

1.2 Simulating Surface Restricted Imaging

While fMRI is a powerful tool for exploring both intrinsic and extrinsic brain activity, it is also costly, usuitable for certain patient populations and limited in temporal resolution [9, 10]. Alternatives, such as MEG and fNIRS, are less expensive, easier to use and capable of higher sampling frequencies than BOLD fMRI [11, 12, 13]. However, they are lacking in spatial localization and signal measurement depth. With a multi-modal approach, it is possible to overcome the limitations of one modality using the capabilities of the other and vice versa. Our lab developed a method using fMRI constrained to the surface layer of cortex to predict deep brain regions as a way of bolstering the capabilites of surface restricted modalities.

Resting state functional connecitvity has previously been studied in our lab to predict independent and distributed brain regions using support vector regression (SVR) [14]. Work by Tenzer et al. (2016) further developed this into a tool for predicting 10 RSNs and six structurally defined regions from fMRI data limited to the cortical surface [15]. The current study further validates the capabilities of this method, applying it to predicting a functionally defined structure. It also assesses if this technique, which relies on resting state functional connectivity, could utilize task data as well as resting state data, potentially opening up the range of study questions that surface-based measurements can address.

1.3 Fusiform Face Area

We chose the fusiform face area (FFA) as the subcortical region to predict for its robust task response and anatomical depth. This functionally defined region responds selectively to faces compared to non-face images and can be identified using a functional localizer task [16]. A typical functional localizer task consists of a block design paradigm during which the subject is presented with epochs of face images or control images (tools, scrambled faces, etc.) with periods of baseline inbetween. The statistical map in Fig. 1.1 was generated from a meta-analysis 116 studies shows the distribution of voxels that show co-activation with FFA [17].

There is evidence of right hemispheric dominance in face perception [18, 19], that has also been verified in fMRI and positron emission tomography (PET) imaging studies [20, 21, 22,

23]. This extends to FFA, which is typically right lateralized both in activation strength and size. While some studies suggest little to no laterality in left handed populations [16, 24], others report the same laterality between left and right handed populations [25]. In this study, we imposed laterality by restricting our target functional region of interest to be the right FFA.

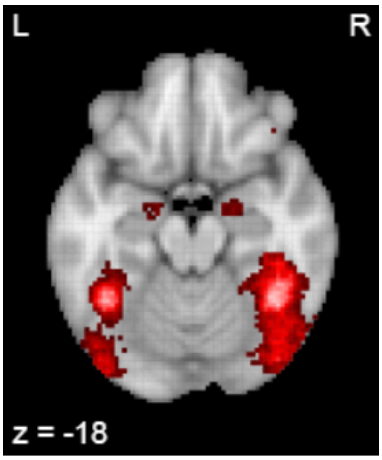

Figure 1.1: **Meta-analysis map of FFA:** Group map of FFA activation generated from 116 studies using the NeuroSynth databaseh [17].

Chapter 2

Methods

2.1 Subjects and Scanning

Each subject completed four functional scans during their session: 2 resting state runs and two functional localizer task runs. Every session started with a resting state scan, while the remaining scans were randomized. This lead to three possible randomizations, illustrated in Fig. 2.1, with possible scan orders for the remaining runs indicated in the dashed boxes. The purpose of collecting two runs of each task was to cross-validate SVR performance within each run type. Prediction accuracies were also cross-validated between run types. Training and testing combinations are also illustrated in Fig. 2.1.

2.2 Resting State

Subjects were instructed to keep their gaze fixated on a static white over black contrasting circle at the center of a gray screen. During the scan, they were asked to let their minds wander and avoid focusing on any particular stream of thought. The scan was performed twice during the entire session, and each run consisted of 166 TR'ss for a duration five minutes and 32 seconds. We a technical error on the presentation screen occured for one subject during 18 seconds before the end of their first resting state scan. The last 10 TRs were censored for this particular run. All other functional runs were typical.

2.3 Functional Localizer Task

Subjects were instructed to keep their gaze fixated on a white over black contrasting circle at the center of the screen. A block design was employed using face and scrambled object

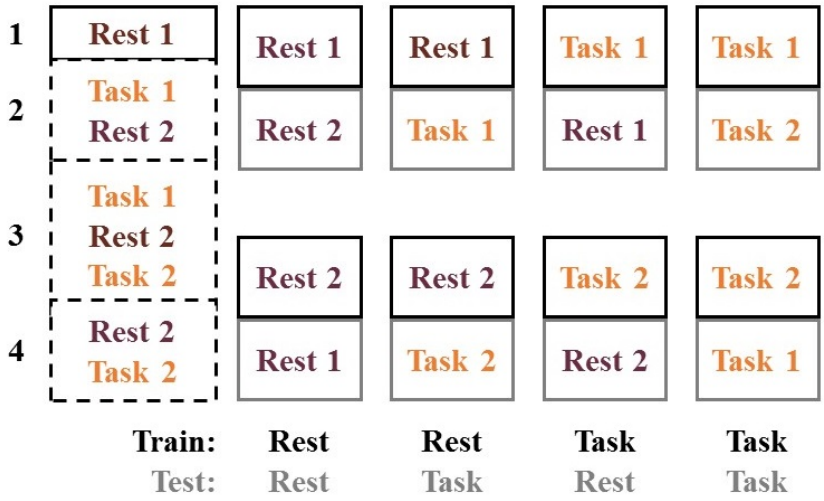

Figure 2.1: **Task order and cross-validation combinations:** The four functional scans are shown on the left, starting with the 1st resting state scan, followed by three randomizations of the second resting state scan and two task scans. The remaining columns represents diagram training and testing run combinations.

images, with epochs of a blank screen inbetween the two conditions [16]. The face stimuli used for this task came from the NimStim set of facial expressions [26] and converted to grayscale, while the scrambled object stimuli were generated in-house from the same set of images using MATLAB. This was to ensure image intensity remained balance across the two conditions. During each block, images randomly selected from the set of stimuli appeared at a rate of once every 0.667 seconds, or 1.5 Hz. The duration of face and object blocks varied from 24-36 seconds, and the duration of the blank blocks varied from 20-24 seconds. The order of face and object blocks was also randomized. To promote vigilence, subjects were also instructed to press a button when they saw the circle at the center of the screen change color from white to red. This occured randomly at an average rate of once every two seconds, or 0.5 Hz. Each run consisted of 166 TR's for a total duration five minutes and 32 seconds.

2.4 Preprocessing

Structural and functional preprocessing were carried out using a combination of tools from AFNI [27] and FSL [28] software packages [14]. After skull stripping and segmentating the antomical images, registration to MNI152 space was performed using a two step approach, which first calculated the linear registration using the FSL's FLIRT tool, then refined this registration using the FNIRT tool [29].

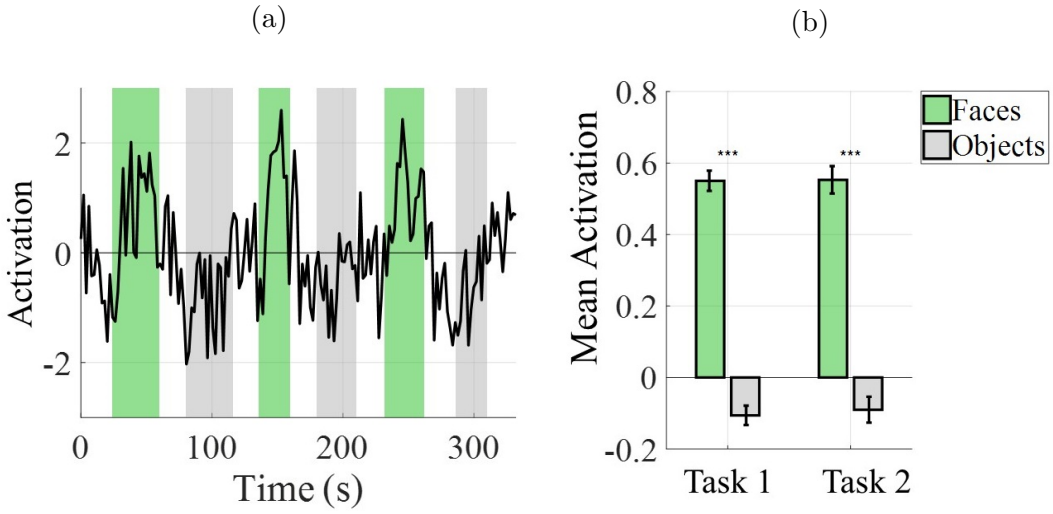

Figure 2.2: **Task activation in right FFA: (a)** Example of time course extracted from right FFA for a single subject. Areas shaded green indicate 'Face' epochs and areas shaded gray indicate 'Object' epochs. **(b)** Average activation for each run during face and object epochs across all subjects ($^{***}p < 0.001$).

Functional data perprocessing began with slice timing and motion correction. Six parameter nuisance regressors were used to calculate subject motion. TRs with motion > 0.5mm were censored. Subjects with a single run containing more than 1.0 mm of motion or required more than 16 TRs to be censored was removed. All volumes was aligned to the third brick of the first run. Surface-based analasyse were performed in native subject space. Next, functional to anatomical alignment and anatomical to MNI152 space transformations were combined and applied to resulting SVR weight maps for second level analysis. In the cases of whole brain and other feature selection conditions, transformation to MNI152 space occured before FFA identification.

2.5 Fusiform Face Area Identification

Functional scans were segmented into two masks: the exterior 10 mm cortex and the remaining interior of the brain. This was done in native space to most accurately capture the spatial geometry of fNIRS limitations. A general linear model (GLM) contrasting between TR's of face blocks and scrambled object blocks was used to identify FFA. To avoid the influence mutual information between SVR models and extracted time courses from FFA, the GLMs of task runs was restricted to the interior of the brain. Peak activations along the right fusiform gyrus were located for each run, and the mean time series from the surrounding 8 mm spherical region were extracted. These mean time series became the *labels* in SVR training and testing. This same procedure was carried out in MNI152 space for whole brain

analysis. The example FFA time course in Fig. 2.2a shows increased activity during green 'Face' blocks compared to grey 'Object' blocks. The mean activation during these blocks across all subjects in Fig. 2.2b shows that activation is significantly higher during 'Face' blocks compared to 'Object' blocks.

2.6 Feature Selection and SVR

Surface based decoding of Fusiform Face area required restricting the *features* used to build support vector regression models to the most superficial 10 millimeters of cortex. Labels extracted from each run were used to train SVR models. Support vector regression training and testing, depicted in Fig. 2.3, were performed on each run using the AFNI plugin 3dsvm [30]: the extracted FFA time series label ($\vec{y}_{train}(t)$) and the surface voxels of the training data ($\vec{x}_{train}(t)$) were used to generate a weight map ($\vec{w}$) to predict the testing label ($y_{test}(t)$) from independent test data ($\vec{x}_{test}(t)$), yielding an estimated time series ($\hat{y}_{test}(t)$). This weight vector $\vec{w}$ can be mapped onto the anatomical brain to localize activation [30] . Accuracy of these models was calculated as the correlation between test labels and the predicted time courses.

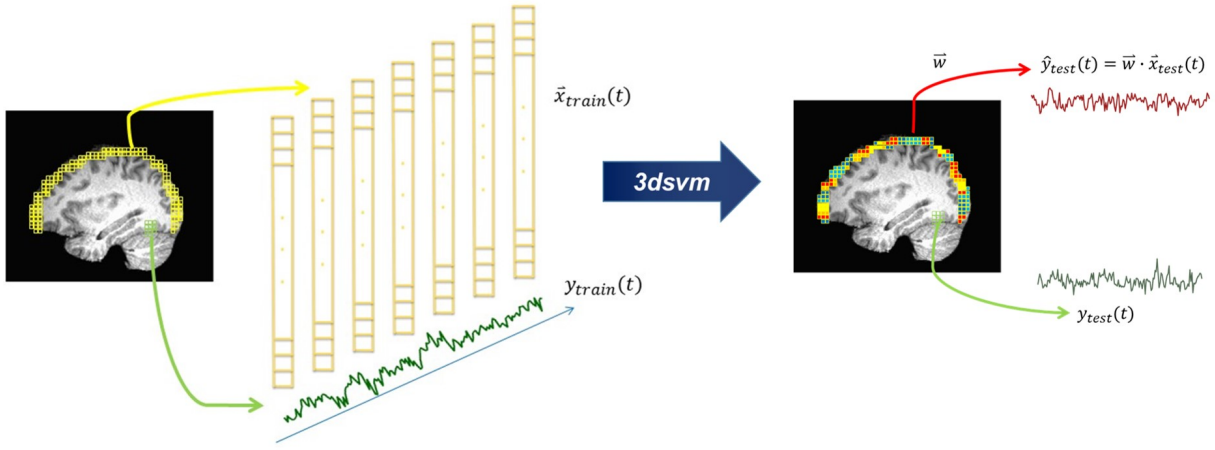

Figure 2.3: **Feature selection and SVR regression:** Voxels in the 10 mm surface layer of cortex (yellow) and the extracted time FFA time course (green) are used as the training data and label in SVR regression to generate a weighted map (multi) to estimate the test label (dark green), yielding a predicted time course (red).

2.7 Null Distribution of prediction accuracy and Reproducibility

Performance of SVR models was compared to chance using a nonparametric prediction, activation, influence, and reproducibility resampling (NPAIRS) framework [14, 31]. Training labels were permuted with the PyWavelet software using 4th order Daubechies wavelets [32] and used to generate SVR predictions based on random chance. For each train-test pair, 1000 wavestrapping permutations (2000 per task combination) were generated to produce null accuracy distributions.

2.8 Statistics

To identify significant activation in group level fMRI analysese, the standard practice of calculating false discovery rate (FDR) corrected group maps was performed using AFNI, thresholding activation at $q<0.05$ [33]. It is necessary in fMRI to use the FDR corrected q-values as opposed to conventional p-values to account for multiple comparisons when performing a statistical test on several thousand voxels individually.

When performing cross validation, the differences in SVR accuracy were tested for significance based on which functional data were used to train and test. For this, ANOVAs were calculated comparing across the four different combinations (Rest-Rest, Rest-Task, Task-Rest, Task-Task) and the p-values were calculated using a paired T-test. Error bars were calculated by taking the standard error of the mean ($\frac{\sigma}{\sqrt{n}}$) for each pairing across 27 subjects.

Chapter 3

Results

3.1 Surface Restricted SVR Decoding of FFA

Three subjects were excluded based on motion. The remaining 27 subjects were used to generate SVR models and predict test labels from the FFA using surface restricted fMRI data. Examples of prediction and test label pairs for each cross-validation combination are shown for a representative subject in Fig. 3.2.

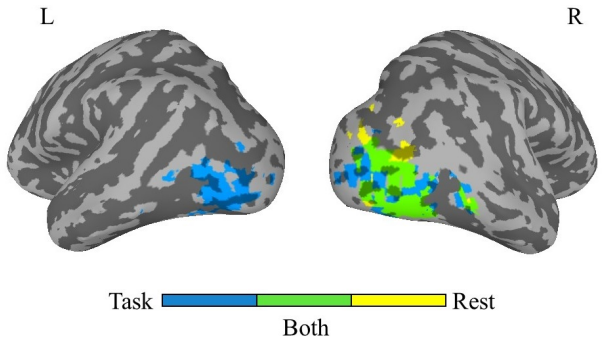

Figure 3.1: **SVR surface weight maps:** SVR weight maps (N=27, p≤0.05) for subjects were generated using both resting state and task data; blue regions are found exclusively in task, yellow regions are found exclusively in Rest, and green represents the overalp of both.

SVR weight maps generated from rest and task were combined into two group maps, then projected onto an inflated anatomical brain using FreeSurfer and SUMA software [34, 35]. Both resting state and task produced overlapping FDR corrected (q<0.05) clusters with a focus point in the right middle occipital gyrus, as shown in Fig. 3.1. The task based map also produced a similar cluster in the left hemisphere, indicating that there may be hemispheric differences in functional connectivity between rest and task. The dominance of

Table 3.1: **Talairach coordinates of clusters.** Foci specified in Talairach LPI coordinates. Peak t values reflect q<0.05 at extent threshold > 25 voxels.

		Coordinates (mm)			
Region	**BA**	**x**	**y**	**z**	**t**
10 mm Surface (Task)					
R Middle Occipital Gyrus		50	-68	-3	6.7
L Inferior Temporal Gyrus		-42	-82	-8	6.1
10 mm Surface (Rest)					
R Middle Occipital Gyrus		50	-68	-10	4.4
Task vs. Rest					
R Inferior Occipital Gyrus	19	42	-76	-6	7.5
L Fusiform Gyurs		-42	-69	-16	7.4
R Lingual Gyrus	18	2	-80	1	-6.8
L, left; R, Right.					

right hemisphereic activation may be the result of imposed laterality by selecting FFA in the right hemisphere. However, we note that these maps do not show statistically significant differences, and at lower statistal threshold, there is bilateral activaiton in the resting state-based group map. The claim of functional connectivity differences between rest and task is, therefore, weak and only pertains to co-activation strength and not location.

Peformance of SVR maps was assessed within and between run types. The bar plots in Fig. 3.3 show prediction accuracy of the surface limited models compared to the whole brain. While whole brain modeling performed slightly better than surface restricted modeling, they both peformed above chance for all cross-validation combinations.

We also noticed a trend in prediction accuracy between 'task' and 'rest' similar to previous work in the lab by Papageorgiou et al. (2013) which compared prediction accuracy between 'control' and 'no control' [36]. In our study, training and testing on 'task' data yielded significantly higher prediction accuracy than other combinations, and in this earlier study, training and testing on runs where subjects had 'control' over the position of a needle yielded higher prediction accuracies. Following a similar procedure, we investigated the influence of spatial SNR on prediction accuracy.

3.2 Prediction Accuracy and Spatial SNR

By taking two statistical brain maps of the same type, it is possible to calculate the spatial signal-to-noise ration (SNR) as outlined by the nonparametric prediction, activation, influence, and reproducibility resampling (NPAIRS) framework [31, 37]. Taking the correlation

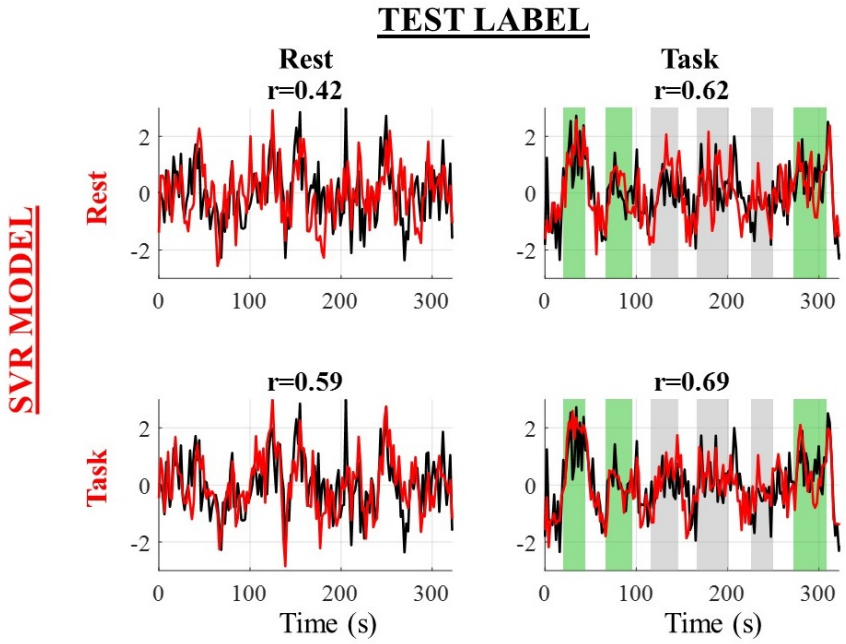

Figure 3.2: **Example of SVR predictions:** Extracted time courses from FFA (black) are overlayed with predicted time courses (red) for each training-testing combinations. Gray and green bars represent 'Object' and 'Face' epochs in during the functional localizer task.

of the two statistical maps yields the matrix in Eq. 3.1, which can be decomposed using principal component analysis (PCA), resulting in singular values $(1 + r)$ and$(1 - r)$ along two eigenvectors.

$$\begin{pmatrix} 1 & r \\ r & 1 \end{pmatrix} = \begin{pmatrix} \frac{1}{\sqrt{2}} & \frac{1}{\sqrt{2}} \\ \frac{1}{\sqrt{2}} & \frac{-1}{\sqrt{2}} \end{pmatrix} \begin{pmatrix} 1+r & 0 \\ 0 & 1-r \end{pmatrix} \begin{pmatrix} \frac{1}{\sqrt{2}} & \frac{1}{\sqrt{2}} \\ \frac{1}{\sqrt{2}} & \frac{-1}{\sqrt{2}} \end{pmatrix} \tag{3.1}$$

The first principal eigenvector defines the signal direction, the second eigenvector is orthogonal to the signal and r is the spatial signal correlation. Assuming a gaussian signal distribution, the noise will be equally present in both directions, allowing us to calculate spatial SNR using the two eigenvalues : $\frac{(1+r)-(1-r)}{1-r} = \frac{2r}{1-r}$. This expression is used to calculate SNR_{Rest} $(\frac{2r_{Rest}}{1-r_{Rest}})$ and SNR_{Task} $(\frac{2r_{Task}}{1-r_{Task}})$.

The difference in SNR between task and rest (ΔSNR = SNR_{Task}− SNR_{Rest}) and prediction accuracy (ΔAaccuracy = Accuracy_{Task}− Accuracy_{Rest}) was for surface restricted SVR models, as well as the whole brain SVR models for comparison. The R^2 values, which describe the percent variance explained betwen ΔSNR and ΔAccuracy, shown in Fig. 3.4a, were about half for whole brain modeling, and about three quarters for surface modeling. To compare surface and whole brain relationships without bias from the number of features, the relationship was also quantified using mean accuracy and mean SNR. in Fig. 3.4b, with

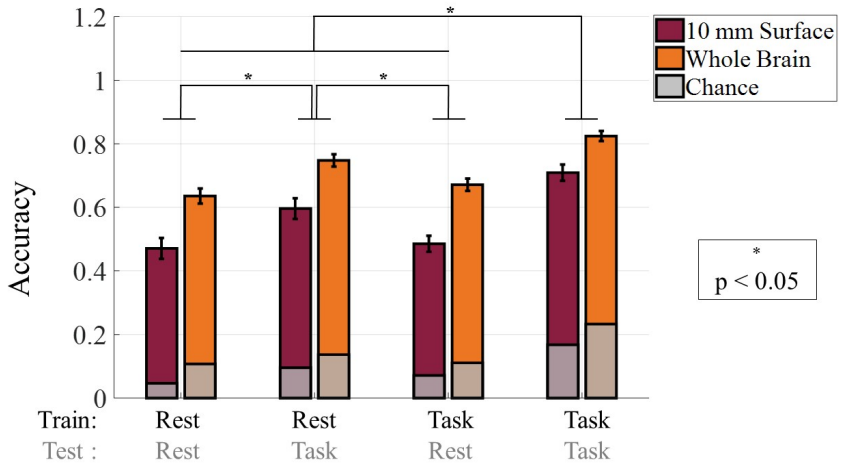

Figure 3.3: **Accuracy of train-test pairs for surface and whole brain analysis:** Results of SVR regression using 10 mm cortical surface (maroon) compared to using the whole brain (orange). All models performed well above chance (gray). Error bars represent standard error of the mean.

R^2 values listed in Table 2. Both surface restricted and whole brain analysese produced R^2 greater than 0.50.

3.3 Modulating SNR through Feature Selection

The results of a mixed effects ANOVA contrasting task and resting state SVR maps, shown in Fig. 3.5, revealed three statistically signifcant regions: two bilateral clusters surrounding the right and left fusiform gyri with higher activation for task and a medial cluster focused on ther right lingual gyrus with higher activation for rest. The relationship between mean SNR and mean accuracy again, this time excluding different combinations task and rest related clusters to disentangle their influences.

The resulting R^2 values reported in Table 3.2 were above 0.50 for all feature selection criteria. The R^2 values from excluding both task related clusters are similar to those from excluding just the ipsilateral (right) cluster. Excluding the contralateral (left) cluster yields R^2 closer to that of the whole brain analysis. Excluding only the rest related cluster also yields R^2 similar to using the whole brain, while excluding all clusters yields results closer to excluding both clusters.

Next, the average accuracies ($\overline{\text{Accuracy}}$) were plotted as a function of average signal to noise ($\overline{\text{SNR}}$) for all feature selection condtions in Fig. 3.6. Averaging between resting state and task in Fig. 3.6a, we observed the following:

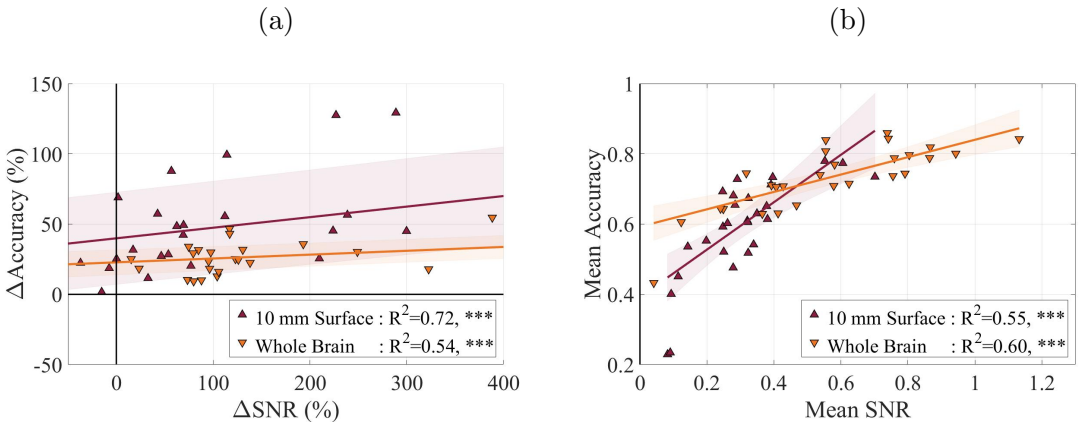

Figure 3.4: **SNR-accuracy relationship: (a)** Regression fit of ΔAccuracy versus ΔSNR for surface and whole brain analyses. **(b)** Regression fit of mean accuracy and mean SNR for surface and whole brain analyses. Shaded regions represent 95% confidence interval.

Table 3.2: **Mean Accuracy - Mean SNR Relationship:** R^2 values reported for all feature selection conditions.

Feature Selection	$\mathbf{R^2}$	p
10 mm Surface	0.55	9.9×10^{-6}
Whole Brain	0.59	2.6×10^{-6}
Exclude Bilateral Cluster	0.58	4.4×10^{-6}
Exclude Right Cluster	0.56	7.5×10^{-6}
Exclude Left Cluster	0.59	2.9×10^{-6}
Exclude Rest Cluster	0.51	2.9×10^{-5}
Exclude All Clusters	0.58	4.5×10^{-6}

1. The 10 mm surface restricted features had the lowest $\overline{\text{SNR}}$ and $\overline{\text{Accuracy}}$.
2. Excluding both task clusters led to a decrease in both variables relative to the whole brain.
3. Excluding the right cluster had a very similar effect to excluding both task clusters, while excluding the left cluster led to $\overline{\text{Accuracy}}$ and $\overline{\text{SNR}}$ closer to the whole brain.
4. Excluding the rest related cluster led to a boost in $\overline{\text{SNR}}$ relative to the whole brain, but not $\overline{\text{Accuracy}}$.
5. Excluding the rest related cluster and task related clusters lead to an increase in $\overline{\text{SNR}}$ relative to excluding just the task related clusters, but not $\overline{\text{Accuracy}}$.

Examening $\overline{\text{SNR}}$ and $\overline{\text{SNR}}$ based on task data in Fig. 3.6b, these same observations listed above are present. There is a difference for rest data, shown in Fig. 3.6c when excluding

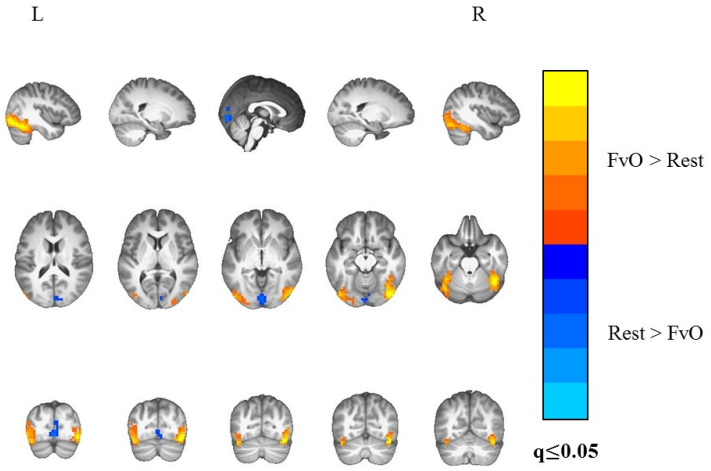

Figure 3.5: **Group map contrast of SVR maps from task task and resting state:** FDR corrected map of mixed effects ANOVA comparing SVR weight maps (N=27, yellow-red = Task>Rest, cyan-blue = Rest>Task, q<0.05).

the left cluster alone. It does not improve the $\overline{\text{SNR}}$ relative to excluding both task clusters. These results show the variability of accuracy and SNR both with respect to regional sources of signal and type of data used in SVR modeling.

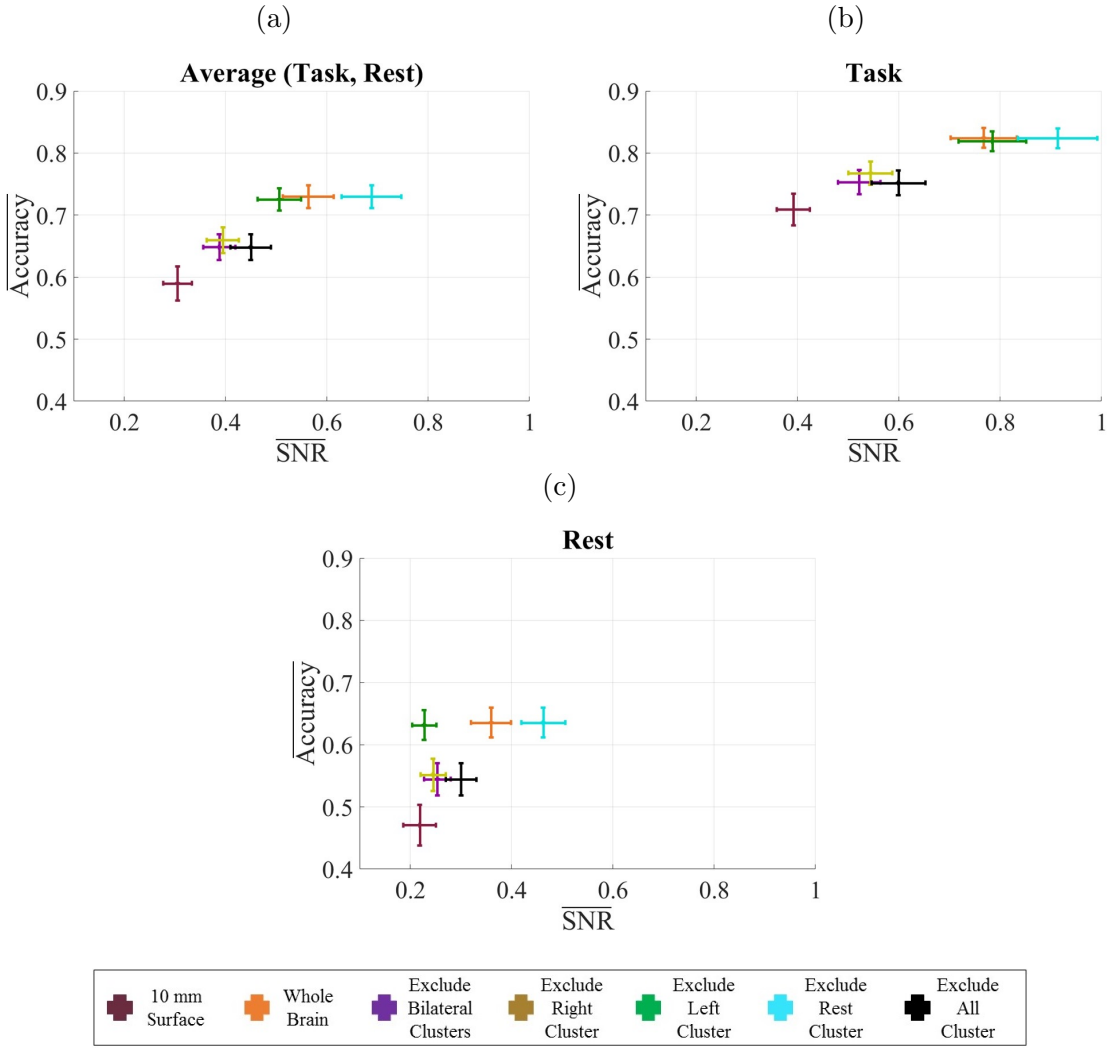

Figure 3.6: **Average SNR and Accuracy of all feature selection conditions:** Plots of $\overline{\text{Accuracy}}$ versus $\overline{\text{SNR}}$ for **(a)** the average of rest and task models, **(b)** task models and **(c)** rest models. A legend at the bottom specifies the feature selection criteria in each plot. Bars represent standard error of the mean.

Chapter 4

Discussion

4.1 Cortical Surface Can Decode FFA in Rest and Task

We met he original objective of this study by successfully predicting right FFA using only surface restricted features. This validates the utility of our previously established method for decoding functionally defined brain region using brain activity within the sampling space of fNIRS. Although it did not perform as well as using the whole brain to predict FFA, the 10 mm cortical surface produced accuracies well above chance. We additionally found that this technique based on resting state connectivity is not unique to rest data, since task data were also able to decode FFA. More so, resting state and task data were interchangeable in predicting each other above chance. This has implications for research using depth-limited neuroimaging, potentially granting them indirect access to deep brain regions linked to distinct cognitive functions using either task or rest data. We also show in Fig 3.1 that while SVR group maps of task data show bilateral activation, resting state group maps only show ipsilateral activation. This suggests a change in functional connectivity between hemispheres when comparing resting state and task based activation, though this difference is not significant.

4.2 Relationship Between SNR and Accuracy

Figure 3.3 shows that training and testing on task results in significantly higher prediction accuracy when compared on other training-testing combinations. We observed an analogous relationship in past work from the lab on brain computer interfaces when cross-validating 'control' and 'no-control' data, where 'control' referred to a participant being able to change the position of a needle on the screen by changing their covert counting speed [36]. This earlier work suggested that a boost in prediction accuracy was the result of a boost in spatial

SNR. While the link between prediction accuracy and SNR has not been fully characterized [31, 37], the work by Papageorgio et al. found evidence of a relationship in variance between ΔSNR and ΔAccuracy. The parallels between the current study and this past study were suprising, but, in hindsight, also makes sense intuitively. Extrinsicly driving brain activity by giving participants control over an interface is similar to driving the brain activity in a participant's FFA by presenting them with face and control images. This lead us to follow the example from this earlier work and use the NPAIRS framework to assess the Accuracy-SNR relationship.

We fit a linear regression between ΔSNR and ΔAccuracy for our study, which we report in Fig. 3.4a, for both surface restricted features and whole brain features. The resulting R^2 was much larger for whole brain than for surface restricted SVR. Since the 10 mm surface volume contained far fewer than that of the whole brain, we wanted to test a slightly different metric which was less prone to bias. We fit a linear regression to the mean SNR and mean accuracy and found the same trend still present, which we have depicted in Fig. 3.4b. Values we obtained for R^2 and significance values for these fits are listed in Table 3.2. These results corroborate the finding by Papageorgiou et al., validating the relationship between spatial SNR and prediction accuracy.

The $\overline{\text{SNR}}$ and $\overline{\text{Accuracy}}$ plots in 3.6 tell similar stories with respect to accuracy. Maximum accuracy was achieved for all cases where the right task cluster was not excluded. Excluding both task clusters performs similarly to excluding both task clusters. This was likely due to the fact that SVR labels were extracted from voxels within the right task cluster, giving this region greater predictive power.

When examining $\overline{\text{SNR}}$, we noticed another trend consistent for Figs. 3.6a, 3.6b and 3.6c. Excluding the rest related cluster, we notice a boost in $\overline{\text{SNR}}$ relative to the whole brain. However, this boost does not result in an increase to $\overline{\text{Accuracy}}$. We found a similar boost in $\overline{\text{SNR}}$ relative to excluding the task related clusters, but again, there was no increase in $\overline{\text{Accuracy}}$.

Lastly, we observe a difference between plots in Fig. 3.6b and Fig. 3.6c. Excluding only the left related cluster boosts SNR for task SVR, but not for rest SVR.

We interpreted these results to mean that while SNR and accuracy are related, the strength of this relationship depends on the functionality (rest related vs. task related) of regions included in feature selection, as well as the type of data (resting state vs. task) used to in SVR modeling.

Bibliography

[1] Seiji Ogawa, Tso-Ming Lee, Alan R Kay, and David W Tank. Brain magnetic resonance imaging with contrast dependent on blood oxygenation. *Proceedings of the National Academy of Sciences*, 87(24):9868–9872, 1990.

[2] Peter A Bandettini. Functional mri limitations and aspirations. In *Neural Correlates of Thinking*, pages 15–38. Springer, 2009.

[3] T Dill. Contraindications to magnetic resonance imaging. *Heart*, 94(7):943–948, 2008.

[4] Ann M Hermundstad, Danielle S Bassett, Kevin S Brown, Elissa M Aminoff, David Clewett, Scott Freeman, Amy Frithsen, Arianne Johnson, Christine M Tipper, Michael B Miller, et al. Structural foundations of resting-state and task-based functional connectivity in the human brain. *Proceedings of the National Academy of Sciences*, 110 (15):6169–6174, 2013.

[5] Catie Chang and Gary H Glover. Time–frequency dynamics of resting-state brain connectivity measured with fmri. *Neuroimage*, 50(1):81–98, 2010.

[6] KJ Friston, CD Frith, PF Liddle, and RSJ Frackowiak. Functional connectivity: the principal-component analysis of large (pet) data sets. *Journal of Cerebral Blood Flow & Metabolism*, 13(1):5–14, 1993.

[7] Bharat Biswal, F Zerrin Yetkin, Victor M Haughton, and James S Hyde. Functional connectivity in the motor cortex of resting human brain using echo-planar mri. *Magnetic resonance in medicine*, 34(4):537–541, 1995.

[8] Stephen M Smith, Peter T Fox, Karla L Miller, David C Glahn, P Mickle Fox, Clare E Mackay, Nicola Filippini, Kate E Watkins, Roberto Toro, Angela R Laird, et al. Correspondence of the brain's functional architecture during activation and rest. *Proceedings of the National Academy of Sciences*, 106(31):13040–13045, 2009.

[9] Nikos K Logothetis. What we can do and what we cannot do with fmri. *Nature*, 453 (7197):869, 2008.

[10] R Todd Constable. Challenges in fmri and its limitations. In *Functional Neuroradiology*, pages 331–344. Springer, 2011.

[11] Yoko Hoshi. Functional near-infrared optical imaging: Utility and limitations in human brain mapping. *Psychophysiology*, 40(4):511–520, 2003.

[12] Marco Ferrari and Valentina Quaresima. A brief review on the history of human functional near-infrared spectroscopy (fnirs) development and fields of application. *Neuroimage*, 63(2):921–935, 2012.

[13] Matti Hämäläinen, Riitta Hari, Risto J Ilmoniemi, Jukka Knuutila, and Olli V Lounasmaa. Magnetoencephalography—theory, instrumentation, and applications to noninvasive studies of the working human brain. *Reviews of modern Physics*, 65(2):413, 1993.

[14] C. Craddock, M. Milham, and S. LaConte. Predicting intrinsic brain activity. *NeuroImage*, 82:127–136, 2013.

[15] M. Tenzer, J. Lisinski, A. Eltahir, and S. Laconte. Decoding the brain's surface to track whole-brain and interior brain activity. In *OHBM 2016*, 2016.

[16] Nancy Kanwisher, Josh McDermott, and Marvin M Chun. The fusiform face area: a module in human extrastriate cortex specialized for face perception. *J. Neurosci.*, 17 (11):4302–4311, 1997.

[17] T Yarkoni, RA Poldrack, TE Nichols, DC Van Essen, and TD Wager. Neurosynth, 2011.

[18] Gillian Rhodes. Lateralized processes in face recognition. *British journal of Psychology*, 76(2):249–271, 1985.

[19] Justine Sergent. Role of the input in visual hemispheric asymmetries. *Psychological bulletin*, 93(3):481, 1983.

[20] Ming Meng, Tharian Cherian, Gaurav Singal, and Pawan Sinha. Lateralization of face processing in the human brain. *Proceedings of the Royal Society of London B: Biological Sciences*, 2012.

[21] Joseph Dien. A tale of two recognition systems: Implications of the fusiform face area and the visual word form area for lateralized object recognition models. *Neuropsychologia*, 47(1):1 – 16, 2009. ISSN 0028-3932.

[22] Bruno Rossion, Laurence Dricot, Anne Devolder, Jean-Michel Bodart, Marc Crommelinck, Beatrice de Gelder, and Richard Zoontjes. Hemispheric asymmetries for whole-based and part-based face processing in the human fusiform gyrus. *Journal of Cognitive Neuroscience*, 12(5):793–802, 2000.

[23] Bruno Rossion, Carrie A Joyce, Garrison W Cottrell, and Michael J Tarr. Early lateralization and orientation tuning for face, word, and object processing in the visual cortex. *NeuroImage*, 20(3):1609 – 1624, 2003.

[24] Roel M. Willems, Marius V. Peelen, and Peter Hagoort. Cerebral lateralization of face-selective and body-selective visual areas depends on handedness. *Cerebral Cortex*, 20 (7):1719–1725, 2010.

[25] Henryk Bukowski, Laurence Dricot, Bernard Hanseeuw, and Bruno Rossion. Cerebral lateralization of face-sensitive areas in left-handers: Only the ffa does not get it right. *Cortex*, 49(9):2583 – 2589, 2013. ISSN 0010-9452.

[26] Nim Tottenham, James W. Tanaka, Andrew C. Leon, Thomas McCarry, Marcella Nurse, Todd A. Hare, David J. Marcus, Alissa Westerlund, BJ Casey, and Charles Nelson. The NimStim set of facial expressions: Judgments from untrained research participants. *Psychiatry Research*, 168(3):242 – 249, 2009.

[27] Robert W Cox. Afni: software for analysis and visualization of functional magnetic resonance neuroimages. *Computers and Biomedical research*, 29(3):162–173, 1996.

[28] Stephen M. Smith, Mark Jenkinson, Mark W. Woolrich, Christian F. Beckmann, Timothy E.J. Behrens, Heidi Johansen-Berg, Peter R. Bannister, Marilena De Luca, Ivana Drobnjak, David E. Flitney, Rami K. Niazy, James Saunders, John Vickers, Yongyue Zhang, Nicola De Stefano, J. Michael Brady, and Paul M. Matthews. Advances in functional and structural mr image analysis and implementation as fsl. *NeuroImage*, 23: S208 – S219, 2004. ISSN 1053-8119. Mathematics in Brain Imaging.

[29] Mark Jenkinson, Peter Bannister, Michael Brady, and Stephen Smith. Improved optimization for the robust and accurate linear registration and motion correction of brain images. *NeuroImage*, 17(2):825 – 841, 2002. ISSN 1053-8119.

[30] S. LaConte, S. Strother, V. Cherkassky, J. Anderson, and X. Hu. Support vector machines for temporal classification of block design fMRI data. *NeuroImage*, 26:317–329, 2005.

[31] Stephen C Strother, Jon Anderson, Lars Kai Hansen, Ulrik Kjems, Rafal Kustra, John Sidtis, Sally Frutiger, Suraj Muley, Stephen LaConte, and David Rottenberg. The quantitative evaluation of functional neuroimaging experiments: the npairs data analysis framework. *NeuroImage*, 15(4):747–771, 2002.

[32] Ed Bullmore, Jalal Fadili, Voichita Maxim, Levent Şendur, Brandon Whitcher, John Suckling, Michael Brammer, and Michael Breakspear. Wavelets and functional magnetic resonance imaging of the human brain. *Neuroimage*, 23:S234–S249, 2004.

[33] Yoav Benjamini and Yosef Hochberg. Controlling the false discovery rate: A practical and powerful approach to multiple testing. *Journal of the Royal Statistical Society. Series B (Methodological)*, 57(1):289–300, 1995. ISSN 00359246.

[34] Anders M Dale, Bruce Fischl, and Martin I Sereno. Cortical surface-based analysis: I. segmentation and surface reconstruction. *Neuroimage*, 9(2):179–194, 1999.

[35] Robert W Cox and Ziad S Saad. Afni, suma, and niml: Interprocess communication in fmri data analysis. *Biomedicine*, 10:171–178, 1997.

[36] T. Dorina Papageorgiou, Jonathan M. Lisinski, Monica A. McHenry, Jason P. White, and Stephen M. LaConte. Brain–computer interfaces increase whole-brain signal to noise. *Proceedings of the National Academy of Sciences*, 110(33):13630–13635, 2013. ISSN 0027-8424.

[37] Stephen LaConte, Jon Anderson, Suraj Muley, James Ashe, Sally Frutiger, Kelly Rehm, Lars Kai Hansen, Essa Yacoub, Xiaoping Hu, David Rottenberg, and Stephen Strother. The evaluation of preprocessing choices in single-subject bold fmri using npairs performance metrics. *NeuroImage*, 18(1):10 – 27, 2003. ISSN 1053-8119.